CHAPTER 2

Effect of TiO_2 Nanorods (TNRs) ETL Thickness on the Performance of FTO/TNRs/$CH_3NH_3PbI_3$/PTAA/Pd Strcuture Based Perovskite Solar Cells*

Contents

*Part of this work has been published as:

1. Jarwal, Deepak Kumar, et al. "Fabrication and TCAD simulation of TiO_2 nanorods electron transport layer based perovskite solar cells." *Superlattices and Microstructures* (2020): 106463.

CHAPTER 2

Effect of TiO_2 Nanorods (TNRs) ETL Thickness on the Performance of FTO/TNRs/$CH_3NH_3PbI_3$/PTAA/Pd Strcuture Based Perovskite Solar Cells

2.1 Introduction

Thin film-based solar cells are getting much attention to meet the global demand for low-cost and clean energy [105], [106]. Recently, thin-film solar cells are dominated by the inorganic-organic hybrid perovskites, which are synthesized and deposited by low-cost solution processing methods [107]-[109]. The hybrid perovskite materials are now synthesized with a high absorbing coefficient, long diffusion length, ambipolar charge transport, tunable bandgap, and low exciton binding energy [110]–[115]. Considerable efforts have been made in the last few years to improve the PCE of the hybrid perovskite solar cells (PSCs) [49]–[52]. The improvement in the PCE has also been achieved by optimizing the thin-film processing technology along with bandgap engineering of the perovskite film in the solar cells [19].

As discussed in Chapter-1, PCE is significantly enhanced by hybrid perovskite or by choosing a suitable wide bandgap material for electron transport layers (ETLs), hole transport layers (HTLs), and bandgap alignment in the device structure. In the hybrid PSCs, TiO_2 and ZnO are widely used materials for the ETL, while PTAA and spiro-OMeTAD are commonly used for the HTL due to their better alignment of energy levels with those of the perovskite materials [9], [20], [21]. The one-dimensional (1-D) nanostructure is preferred over their bulk counterparts for ETL, as discussed in Chapter-1. The 1-D TiO_2 NRs (TNRs) provide the direct path for the charge carrier transport,

thereby enhancing the carrier transportation by nearly 50 to 80 times that obtained in nanoparticles and other nanostructures [27], [28]. Further, TNR also provides enhanced chemical and mechanical stability for the perovskite solar cell structures [28]. Moreover, the low-cost solution processing techniques [28]–[30] are preferred for the large area growth of NRAs.

It is observed from the literature survey discussed in Chapter-1 that no systematic investigations are carried out for the effect of TNRs transport layer thickness on the performance of PSCs. Furthermore, PSCs' performance optimization for different parameters (i.e., dimensional or material) using the computer-aided design (CAD) simulation tool will be an added advantage for practical feasibility, time effectiveness, and cost-cutting. Fabrication and simulation of a Pd/PTAA/hybrid perovskite ($CH_3NH_3PbI_3$)/TiO_2 nanorods (TNRs) based PSC is carried out on an FTO coated glass substrate in this chapter. The CH_3NH_3I (Perovskite), TNRs, and PTAA layers act as active, ETL, and HTL, respectively. Three devices have been considered with three different TNRs based ETL thicknesses. The PSC devices have been fabricated by a chemical solution method in an open environment condition. Measurements have also been carried out in the open atmospheric condition to demonstrate the performance of the PSCs under robust conditions. The measured experimental results for as-fabricated PSCs have been compared with the SCAPS-1D simulation tool to show the difference between the results obtained under the practical and ideal conditions. The content of the rest of this chapter is outlined as follows:

Section 2.2 presents the experimental details for the fabrication techniques for PSCs. Section 2.3 deals with the methodology and process for the numerical simulation of the PSCs. Further, the detailed results and discussion for the fabricated and simulated PSCs

are presented in Section 2.4. Finally, the finding and observations of this chapter are summarized in Section 2.5.

2.2 Experimental Details

The fabrication techniques for the perovskite thin films and the PSCs are presented in this section.

2.2.1 Material Used

All chemicals used in the PSCs fabrication were of analytical grade and used directly without any further purification. The materials, PTAA, PbI_2, and FTO coated substrate, were purchased from Ossila (UK). Titanium (IV) isopropoxide (TTIP), titanium tetrachloride ($TiCl_4$), dimethylformamide (DMF), hydroiodic acid (HI, 55–58 wt%), methylamine (40 wt%), and hydrochloric acid (HCl, 37 wt%) were purchased from Fisher Scientific.

2.2.2 TiO_2 Nanorods Synthesis and $TiCl_4$ Treatment

The synthesis of TiO_2 nanorods was done by a facile hydrothermal method. First of all, fluorine-doped tin oxide (FTO) substrate (15×15 mm^2) was cleaned using a soap solution, acetone, and isopropanol in an ultrasonic bath for 15 minutes, respectively. After that, the cleaned FTO substrate was placed in a tilted position (FTO in the downward direction) in Teflon lined cylinder. Now the solutions of 560 µl TTIP, 30 ml HCl (35%) and 30 ml DI water prepared separately were poured into a Teflon lined cylinder. The cylinder was then sealed properly and kept in a digital muffle furnace (Escon lab. Inst, India) at 180°C. By this method, three types of TNRs samples were prepared of different thicknesses by varying the growth time in the order of 3.5 hour, 5 hour, and 7 hour. The length and diameter of TNRs depend on growth temperature and

time. After the cooling at room temperature, the substrate was rinsed in DI water and then washed with ethanol to remove acids and other impurities. Subsequently, the substrate was annealed at 400°C for 1 hour in the air for a proper crystalline TiO_2 layer. The prepared TNRs sample was post-treated in 40 mM aqueous solution of $TiCl_4$ prepared by dissolving 0.5 ml $TiCl_4$ in 100 ml deionized (DI) water at 80°C for 90 minutes [116]. The $TiCl_4$ treatment helps in the minimization of voids and traps in synthesized TNRs ETL [116]. Finally, the sample was annealed at 450°C for 1 hour.

2.2.3 CH_3NH_3I Perovskite Synthesis

The perovskite precursor CH_3NH_3I (MAI) was synthesized by reacting 15.5 mL HI acid (55–58 wt% aqueous solution) and 13 ml methylamine (40 wt%) in an ice bath while stirring up to 4 hours [117]. The light-yellow color product was obtained after vacuum evaporation at 45^oC, followed by washing four times with diethyl ether. Finally, the light-yellow color powder was converted into white color crystalline powder after drying for 48 hours in a vacuum oven at room temperature.

2.2.4 Device Fabrication

The whole PSCs fabrication was carried out under an open-air atmosphere at a relative humidity of 60% measured by a commercially available hygrometer. The hybrid perovskite thin film was deposited via two-step spin coating methods on $TiCl_4$ treated TNRs samples. 10 mg CH_3NH_3I and 462 mg PbI_2 were dissolved in 1 ml isopropanol and 1 ml DMF, respectively, for the perovskite precursor [116]. In the first step, synthesized CH_3NH_3I was deposited on $TiCl_4$ treated TNRs via spin coating at 3000 rpm for 30 seconds, and then the sample was transferred upon the hot plate to anneal for 10 minutes at 70^0 C. In the second step, PbI_2 was spin-coated for 30 seconds at 3000 rpm. Subsequently, a 20 µl solution of toluene was also spin-coated for fully

crystalline perovskite film and then annealed at 90^0C for 1 hour to obtain a thickness of 350 nm. The 100 nm PTAA was deposited as HTL on perovskite film at 2000 rpm for 30 seconds. Finally, 80 nm top electrode palladium was thermally deposited on HTL. The block diagram of the fabricated PSC structure is shown in figure 2.1 (a). The possible band diagram for the PSC device structure is shown in figure 2.1 (b).

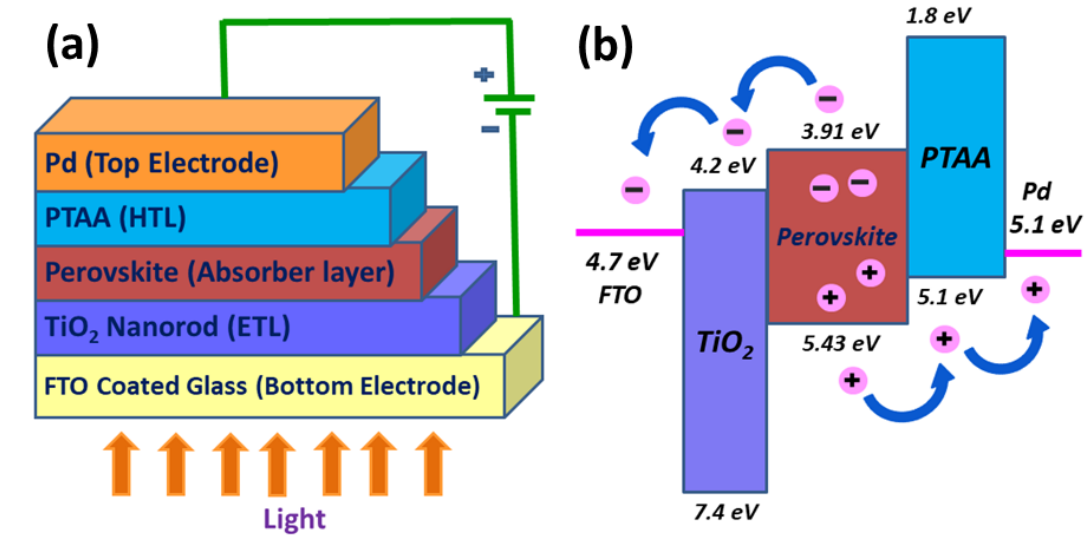

Figure 2.1: (a) Device structure of the PSCs; (b) Band diagram for the fabricated PSCs structure under equilibrium.

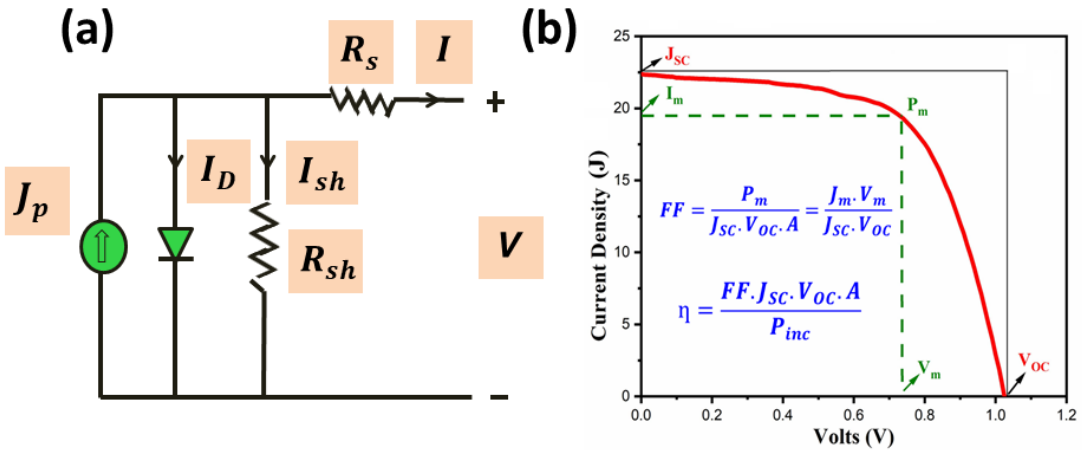

Figure 2.2: (a) Equivalent circuit of perovskite solar cell; (b) Equivalent *J-V* characteristic and performance parameters of PSC.

2.3 Numerical Modeling and Device Simulation

The investigated PSC device is analyzed using the simplified equivalent circuit with

solar parameters shown in figure 2.2 (a) and (b). The governing current density-voltage (*J-V*) equation under dark and Sun-light is expressed as [118]:

$$J = J_0\{\exp[(q(v - JR_S))/\eta K_B T] - 1\} + \frac{V - JR_S}{R_{Sh}} - J_{ph} \quad (2.1)$$

where, J_0, q, η, K_B, R_S, R_{Sh} are the reverse saturation current density, carrier charge, ideality factor, Boltzmann constant, series resistance, and shunt resistance, respectively. T and J_{ph} are the temperature and photon current density.

The 1D TCAD simulation has used the drift-diffusion and Shockley-Read-Hall (SRH) recombination models for computing recombination, trapping, doping, and electric field distribution in the device [119]-[120]. In a hybrid perovskite solar cell, the output current is a result of the diffusion and drift phenomenon of electrons and holes. The light absorbance is calculated by the transfer matrix methods. The drift-diffusion equations for holes and electrons are given as [121]:

$$J_p = J_p(diff) + J_p(drift) = q\left[\mu_p pE - D_p \frac{\partial p}{\partial x}\right] \quad (2.2)$$

$$J_n = J_n(diff) + J_n(drift) = q\left[\mu_n nE - D_n \frac{\partial n}{\partial x}\right] \quad (2.3)$$

where the μ_p and μ_n are electron and hole mobility, D_n and D_p are electron and hole diffusion constants while E is the electric field in the active layer defined by

$$E = \frac{V - V_{bi}}{d}$$

Where V and V_{bi} are the biasing voltage and built-in potential across the ETL/Active layer junction, and d is the thickness of the active layer.

The continuity equations for holes and electrons under illuminated conditions are given

by [33]:

$$q\frac{\partial n}{\partial t}=\left[\nabla \vec{J}_n+qG_n-qR_n\right] \tag{2.4}$$

$$q\frac{\partial p}{\partial t}=\left[\nabla \vec{J}_p+qG_p-qR_p\right] \tag{2.5}$$

For steady-state condition $\frac{\partial p}{\partial t}=\frac{\partial n}{\partial t}=0$, so we have

$$\nabla \vec{J}_n+qG_n=qR_n \tag{2.6}$$

And $$\nabla \vec{J}_p+qG_p=qR_p \tag{2.7}$$

where $G_n(R_n)$ and $G_p(R_p)$ are the electron generation (recombination) and hole generation (recombination) rates, respectively.

To include the effects of defects and traps in various materials on the performance of the PSCs, we have used the SRH recombination model defined by [45].:

$$R=\frac{n.p-n_{\text{int}}^2}{\tau_p(n+n_t)+\tau_n(p+p_t)} \tag{2.8}$$

where τ_p and τ_n are the mean lifetime of the holes and electrons, respectively; R is the recombination rate of the charge carriers; and n_t (p_t) is electron (hole) trap density.

The parameters used for the numerical simulation are listed in Table 2.1. The charge generation rate in the absorbing layer under 1 sun is considered. The amplitude of light intensity in different layers is formulated by using the transfer matrix method, where light intensity, $I(x,\lambda)$, is modeled as a function of position and wavelength. The short-circuit current can be described as [45]:

$$I_{SC,\max}=\iint q\frac{Q(x,\lambda)}{h\upsilon}.dx.d\lambda \tag{2.9}$$

where $Q(x,\lambda)$ is dissipated power per meter square, which can be expressed as

$$Q(x,\lambda)=\alpha(\lambda).I(x,\lambda) \tag{2.10}$$

where α is the absorption coefficient.

The maximum short circuit current ($I_{SC,\ max}$) enumerates us a rough idea for the optimization of layer thickness without affecting the charge transport phenomena in the drift-diffusion model. Maximization of the photon absorption profile in the drift-diffusion model for a particular layer thickness can also be performed to make it more robust. With the help of the photon absorption profile, the generation function for the charge or the exciton continuity equation can be designed depending on the type of solar cell under study.

Table 2.1. The Material Parameters for Numerical Simulation.

Parameter and Units	**TiO_2 NRs** [69], [122]-[124]	**Perovskite** [125]-[127]	**PTAA** [125]
Dielectric Constant (ε_r)	9.0	10	3
Bandgap (eV)	3.2	1.52	3.3
Electron affinity (χ)	4	3.85	2.30
Electron Mobility (μ_n)- $cm^{-2}V^{-1}s^{-1}$	100	2.2	0.002
Hole Mobility (μ_p)- $cm^{-2}V^{-1}s^{-1}$	25	2.2	0.004
CB effective density of states (N_C) (cm^{-3})	2×10^{18}	3×10^{18}	2.2×10^{18}
VB effective density of states (N_V) (cm^{-3})	1.8×10^{18}	3.97×10^{18}	1.8×10^{19}
Electron thermal velocity (cm/s)	1×10^{7}	1×10^{7}	1×10^{7}
Hole thermal velocity (cm/s)	1×10^{7}	1×10^{7}	1×10^{7}

2.4 Results and Discussion

In this section, optical and electrical characterizations of fabricated as well as simulated devices with various thickness variations are presented.

2.4.1 Thin Film Characterization

The hydrothermally grown TNRs samples are first investigated for morphology/composition and crystalline structure using high-resolution scanning emission microscopy (Nova Nano SEM 450, FEI, USA) with in-situ energy dispersion spectroscopy (EDS) (EDAX Inc.) and X-ray diffractometer (XRD, Miniflex, Rigaku, Japan) respectively. The photoemission spectra of perovskite thin film is measured using photoluminescence (PL) spectroscopy (FLS 980 from Edinburgh Instruments, UK). The optical absorption in TNRs and perovskite thin film has been measured using a thin film analyzer (from Filmetrics, USA).

It is found that the grown TNRs have uniform distribution on the surface, as shown in figure 2.3 (a), and desire elemental composition, as shown in figure 2.3 (b). The optimized TNRs with a growth time of 3.5 hour having an average length and average diameter around ~500 nm and ~70 nm were observed from the HRSEM image. The XRD patterns also confirm the formation of good quality crystalline TNRs with mostly rutile phase, as shown in figure 2.4 (a). The perovskite film exhibits single peak emission spectra at an excitation wavelength of 450 nm, as shown in figure 2.4 (b). The morphology of perovskite film on the TNRs is shown in figure 2.5 (a). The cross-sectional image is taken to analyze the thickness of individual layers of FTO/TNRs/Perovskite structure. It is found that the TNRs have an average length of 500 nm and perovskite film has a thickness of ~350 nm, as shown in figure 2.5 (b).

The optical absorption in the optimized TNRs is shown in figure 2.6 (a), which is

comparable to the simulated absorption spectra obtained in the SCAPS-1D simulation tool. It is found that the optical band gap (Eg) and absorbance coefficient (α) have a relation obtained from the tau plot as below [128]:

$$\alpha h\upsilon = A\left(h\upsilon - E_g\right)^m \tag{2.11}$$

where $\alpha = 2.33\log\left(T/d\right)$, T is transmittance, d is the sample thickness, $h\upsilon$ = *1240(incident light (nm))*, and m is a constant. The bandgap of the TNRs is estimated as ~3.2 eV from the experimentally obtained transmittance. The experimental and simulation absorbance spectra of the perovskite layer are shown in figure 2.6 (b).

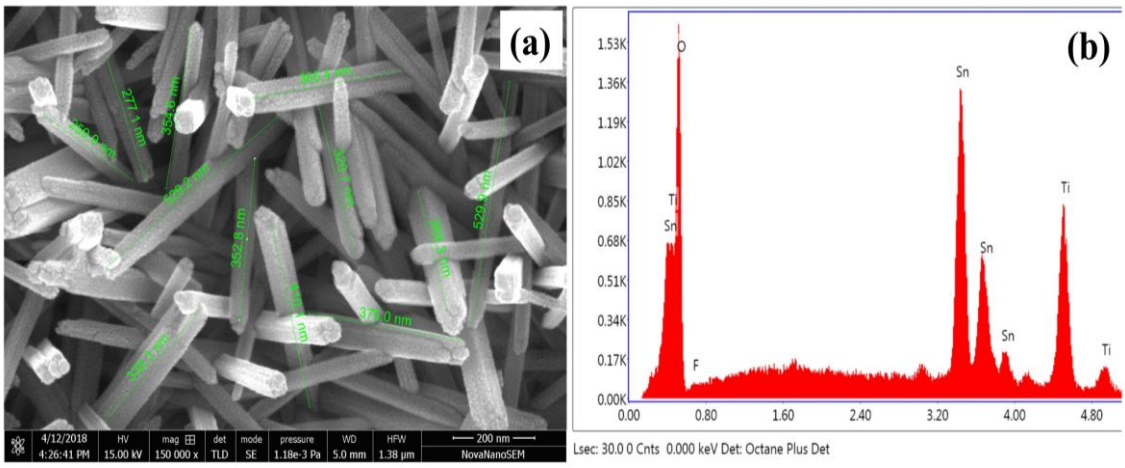

Figure 2.3: (a) HRSEM image of TNRs and (b) EDS image of TNRs.

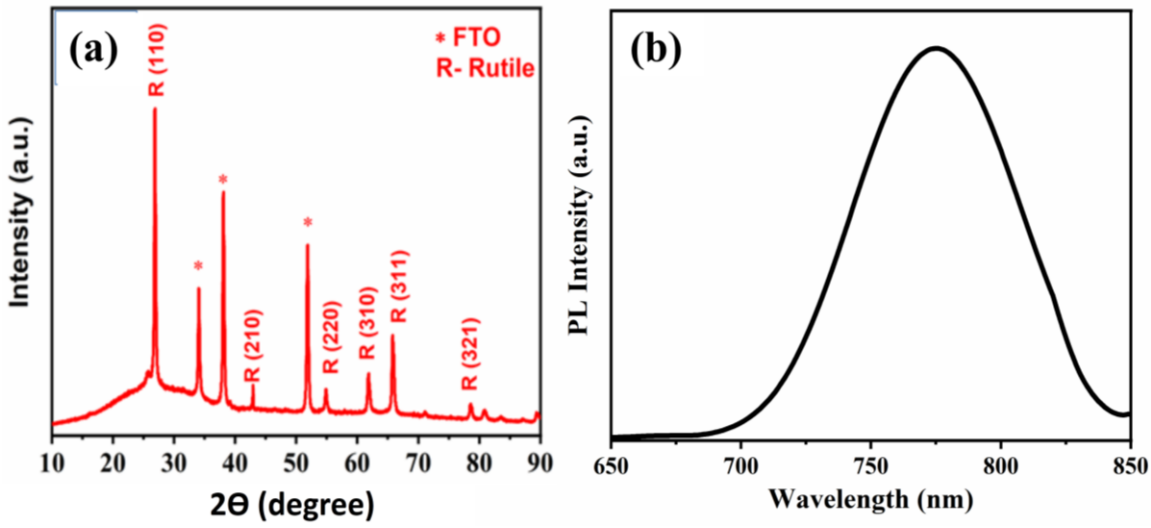

Figure 2.4: (a) XRD pattern of hydrothermally synthesized TNRs and (b) PL emission spectra of perovskite thin film.

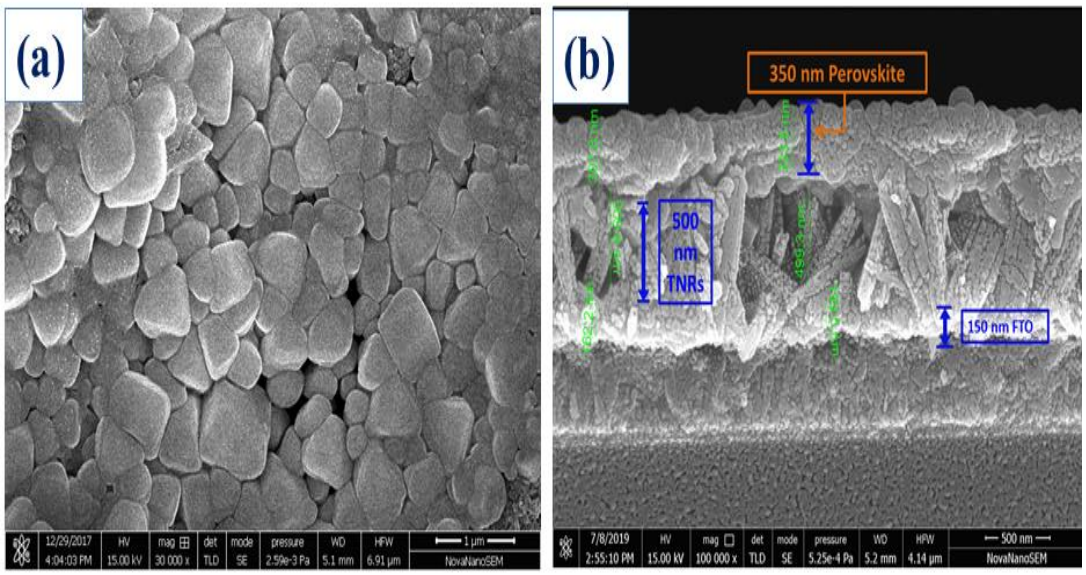

Figure 2.5: HRSEM image of (a) perovskite thin film surface (b) Cross-sectional view of PSC structure without metal electrode.

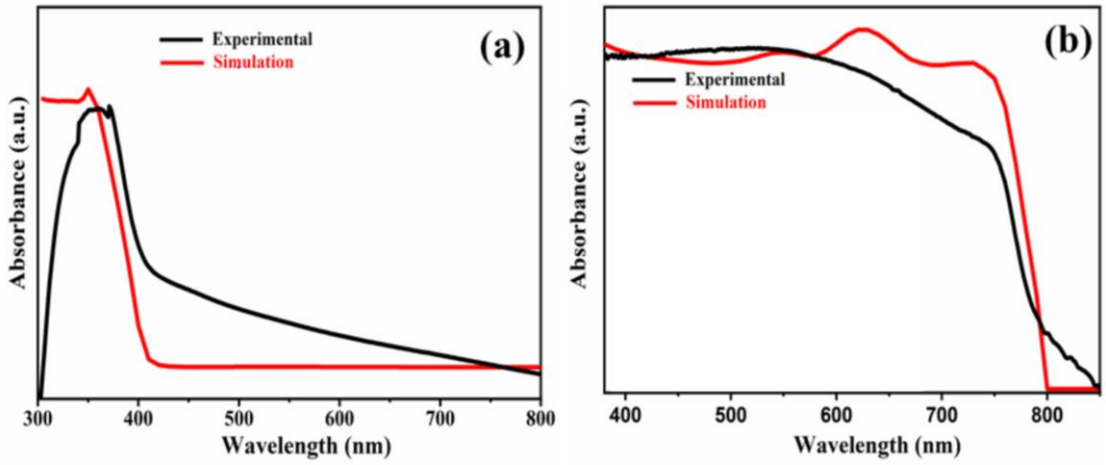

Figure 2.6: (a) Absorbance spectra of hydrothermally synthesized and simulated TNRs on FTO coated glass substrate, (b) Absorbance spectra of synthesized and simulated perovskite thin film.

2.4.2 Solar Cell Characterization

The current density (*J*)-voltage (*V*) characteristics of the fabricated PSCs have been compared with the simulation results in figure 2.7 (a)-(c) for different thicknesses of the TNRs-based ETL of the device. The standard solar light is obtained from the solar simulator (AAA150 from PET, USA). The solar cell parameters *(J_{SC}, V_{OC}, FF,* and *η)* and external quantum efficiency (EQE) are obtained from the *J-V* characteristics. The

TNRs with smaller lengths in the ETL reduce the shunt resistance (which, in turn, increases the dark current) while larger lengths of TNRs enhance the recombination of the photo-generated carriers (which, in turn, reduces the photocurrent) [129], [130]. It is observed that TNRs with lengths ~500 nm result in optimum performance in PSCs considered in the present study. The efficiencies for 200, 350, 500, 650, and 800 nm lengths of TNRs are measured as 13.47, 14.65, 15.04, 11.70, and 10.73%, respectively, in ambient conditions. The efficiencies are slightly lower than other reported works for measurements under a robust open-air atmosphere [131]. A part of perovskite materials breaks into lead iodide and methylammonium iodide in the presence of atmospheric moisture, which limits the efficiency of the PSCs [132]. We have carried out the measurements in the open atmosphere to demonstrate the operation of the PSCs in actual conditions rather under controlled environments. The experimentally estimated performance parameters are compared with the corresponding values obtained from the simulated results in Table 2.2. The simulation results are found to be in close proximity to the experimental data. It may be noted from Table 2.2 that J_{SC} is decreased with increased thickness of the TNRs-based ETL layer due to the possible increase in the series resistance of the solar cell. The open-circuit voltage is reduced from 1.06 ± 0.01 V to 0.95±0.02 V when the thickness of the ETL is increased from 500 nm to 800 nm, possibly due to enhancement in the recombination of charge carriers in nanorods or limitation of diffusion length of charge carriers. As a consequence, overall, the *PCE* is decreased with the increase in ETL layer thickness above 500 nm. Further, the thickness of different layers changes the electric field in the layers, which, in turn, affects the drift current of the device. The diffusion current also depends on the thickness of the active layer. If the thickness of the active layer is less than the diffusion length of the electron (hole), all photo-generated electrons (holes) contribute to the diffusion current.

Otherwise, a part of the photo-generated carriers is lost due to recombination, which affects the device performance.

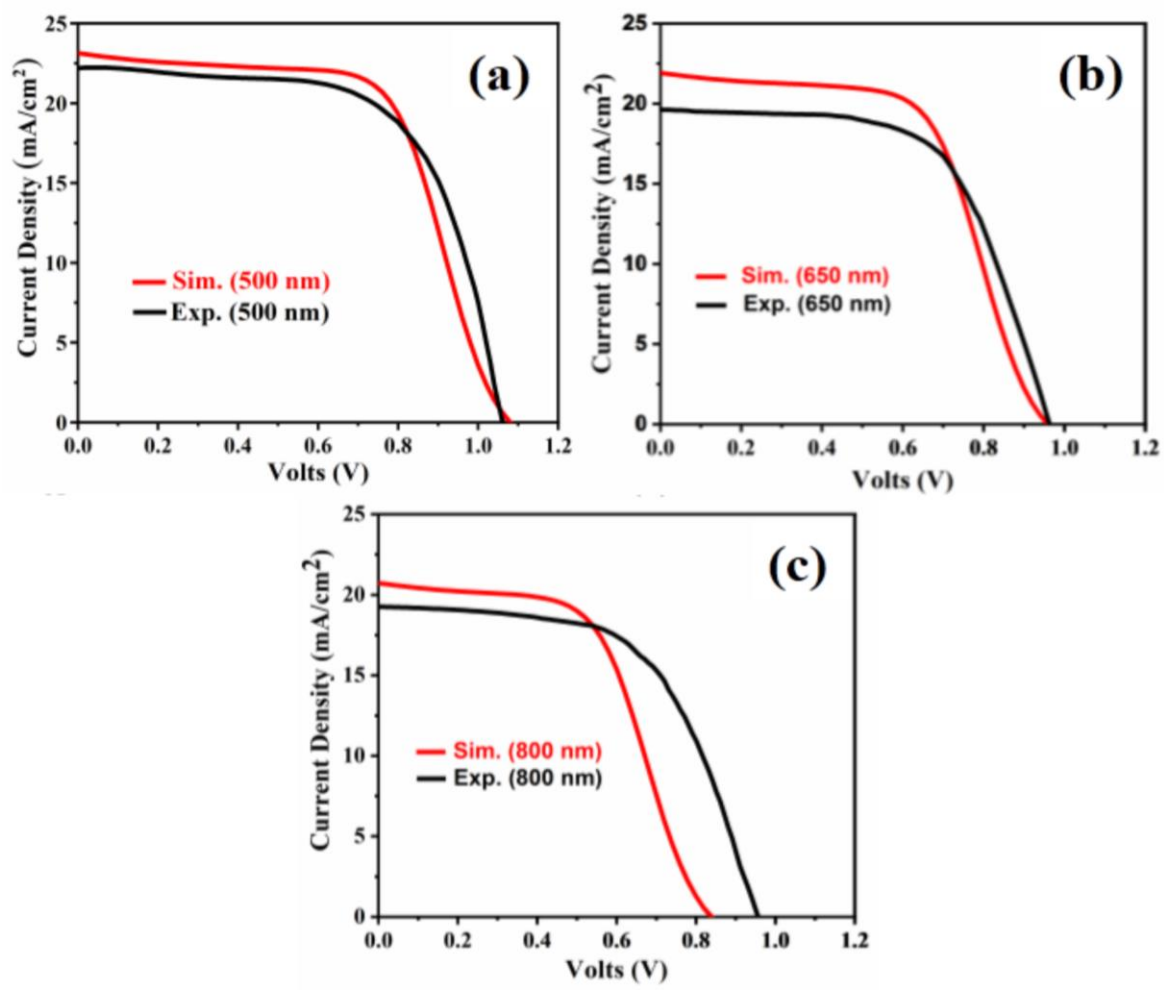

Figure 2.7: J-V curve of fabricated and simulated PSCs with (a) 500 nm TNRs, (b) 650 nm TNRs, (c) 800 nm TNR.

Table 2.2 shows that the current density decreases when the ETL thickness increases. The increase in the ETL thickness decreases the light intensity entering into the active layer, which reduces the photon absorption and hence increases the series resistance of the solar cell. The open-circuit voltage of the solar cell is given by [45]:

$$V_{OC} = \frac{KT}{q}\ln(\frac{J_{SC}}{J_0}) \tag{2.12}$$

The increased ETL thickness enhances the recombination of carriers. This increases J_0 and reduces V_{OC}. Thus, internal power consumption increases with increased ETL

thickness, which affects the fill factor (FF) and the PCE (η) of the PSC. The relationship between FF and PCE is given by [133]:

$$FF = \frac{P_m}{J_{SC}.V_{OC}.A} = \frac{J_m.V_m}{J_{SC}.V_{OC}} \tag{2.13}$$

$$\eta = \frac{FF.J_{SC}.V_{OC}.A}{P_{in}} \tag{2.14}$$

where P_{in} is the incident power from the solar simulator, A is the area of the top electrode of the fabricated PSC and J_m, V_m, and P_m are the maximum current density, maximum voltage, and maximum power obtained from the device. The thickness of the ETL needs to be chosen in such a way that the diffusion length of charge carriers is larger than the thickness of the ETL. For high power conversion efficiency, a 500 nm optimum thickness of ETL is obtained for our proposed structure.

Table 2.2. Fabricated and Simulated Results for Different ETL of the PSCs

		ETL Thickness (nm)		**Performance Parameters**			
ETL Defect Density ($1/cm^3$)	Active Layer Defect Density ($1/cm^3$)	(TNRs Growth Time)		V_{OC}	J_{SC}	FF	η
10^{13}	10^7	500 (3.5 Hour)	Exp.	1.06 ± 0.01	22.19 ± 0.2	0.63±0.01	15.04±0.03
			Sim.	1.07	23.71	0.63	15.69
10^{14}	10^8	650 (5 Hour)	Exp.	0.96±0.02	19.62±0.2	0.62±0.01	11.70±0.05
			Sim.	0.96	21.91	0.59	12.58
10^{15}	10^9	800 (7 Hour)	Exp.	0.95±0.02	19.26±0.2	0.58±0.02	10.73±0.05
			Sim.	0.84	20.71	0.55	9.67

The EQE is computed by the following expression [134]:

$$EQE = 1240 \times \frac{R}{\lambda} \times 100 \tag{2.15}$$

where R is the responsivity defined as

$$R = \frac{I_{Ph}}{P_{in}} \tag{2.16}$$

where P_{in} and I_{Ph} are incident power and output photocurrent of the device at the wavelength λ of the incident light. The external quantum efficiency (EQE) of the fabricated and simulated device is compared in figure 2.8. A close matching is observed for the optimized thicknesses of 500 nm, 100 nm, and 350 nm of the ETL, HTL, and active layers, respectively.

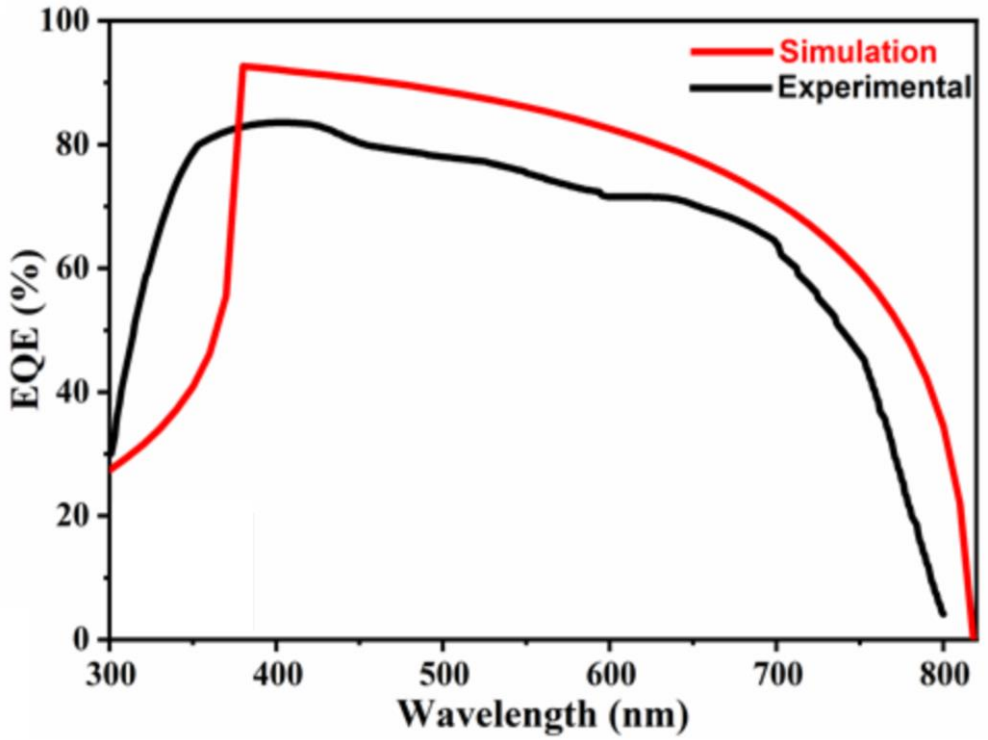

Figure 2.8: External quantum efficiency of fabricated and simulated PSCs with 500 nm ETL, 350 nm active layer, and 100 nm HTL.

2.5 Conclusion

This chapter examines the FTO/TNRs/Perovskite/PTAA/Pd structure-based PSC, where

TNR acts as the ETL, PTAA as the HTL, and hybrid perovskite ($CH_3NH_3PbI_3$) as the active layer of the device. The effects of TNRs thickness on the performance parameters have been investigated using fabricated and simulated solar cells. The morphological, structural, electrical, and optical properties of FTO/TNRs/Perovskite/PTAA/Pd structure have been analyzed for their suitability in solar cell applications. The simulation tool has been explored for optimizing various parameters of the PSC. All the experimental measurements have been carried out in the ambient-air condition. The PCE of the PSC is observed to be decreased for ETL thickness above 500 nm. The optimum values of the PSC parameters V_{OC}, J_{SC}, FF, and PCE are obtained for the thicknesses of 500 nm, 100 nm, and 350 nm of the ETL, HTL, and the active layer, respectively. Optimized simulated values of J_{SC}, V_{OC}, FF, and PCE are obtained as 23.71 mA/cm^2, 1.07 V, 0.63, and 15.69%, respectively, against their corresponding experimentally measured values of 22.19 mA/cm^2, 1.06 V, 0.63, and 15.04%, respectively for the aforementioned optimized thicknesses of the ETL, HTL, and the active layer. The EQE of the simulated and experimental devices matches well for the optimum values of different layers. The close proximity of the simulated electrical and optical characteristics with the experimental results confirms that the TCAD tools can be effectively explored for other PSC structures. The result shows that TNRs thickness also plays a very significant role in the solar cells performance.